



Enhanced removal of arsenic from aqueous solution by novel red mud porous beads: batch and column experiments

Yuxing Xu, Yue Yin , Mengyan Guo, Gaoyang Xu, Linlin Li and Changqing Liu 

School of Environmental and Municipal Engineering, Qingdao University of Technology, Qingdao 266033, PR China

*Corresponding author. E-mail: lcqlyqut@126.com

 YY, 0000-0001-6309-8605; CL, 0000-0002-6114-3238

ABSTRACT

Arsenic contamination in groundwater and rivers has become a major problem around the world, and may cause severe environment pollution and human health problems. In this study, cost-efficient adsorbent red mud porous beads (RPB), using red mud – a kind of alumina industry by-product, was synthesized for adsorptive removal of arsenic(V) from aqueous solution. Kinetic studies showed that chemisorption mainly governed the adsorption process. The experimental data were fitted well using the Langmuir isotherm, and the equilibrium adsorption capacity for arsenic of 11.758 mg/g at pH = 7 conditions. The effect of pH showed that the pH_{pzc} of RPB was 6.0 and at pH = 6 the removal rate reached nearly 100%. The removal rate decreased from 91.3% to 79.0% with increase in the initial concentration of arsenic from 2.5 to 20 mg/L. The adsorption performance from column studies illustrated that the velocity of flow and the initial concentration influenced the breakthrough time of the column. This study would facilitate the use of red mud, which can be fabricated into RPB, acting as a valuable adsorbent for removing arsenic in aqueous solutions.

Key words: adsorption, arsenic, column experiments, porous beads, red mud

HIGHLIGHTS

- RPB was used as a valuable adsorbent for arsenic adsorption.
- Chemisorption governed the adsorption process.
- The experimental data were described well by Langmuir isotherm.
- The velocity of flow and initial concentration influenced the breakthrough time.

INTRODUCTION

Toxic arsenic presented in groundwater and rivers is considered to be a potential issue for the environment and human health (Amen *et al.* 2020). It is reported that long-term exposure to arsenic can induce complications in assorted organ systems of human body comprehensively, even cancer of skin, lung and urinary bladder (Mazumder 2008; Mohammed Abdul *et al.* 2015a). The main source of arsenic in the environment is geological or via anthropogenic activities (Mohammed Abdul *et al.* 2015b). At this time, it has been reported that over 19 million people are drinking from arsenic-polluted water resources in Bangladesh which have a arsenic concentrations above 50 µg/L (Saha *et al.* 2020). However, the safe limit for arsenic in drinking water has been already lowered to 10 µg/L set by the World Health Organization (WHO) in 2008 (WHO, 2008; Akin *et al.*, 2012; Niazi *et al.*, 2018a). Hence, it is of great importance to address the arsenic-polluted water resource issue.

Various processes have been implemented to remove arsenic from drinking water, such as ion exchange, photocatalysis, coagulation/flocculation, electrochemical techniques, and membrane separation (Kim *et al.*, 2003; Bilici Baskan & Pala, 2010; Wan *et al.*, 2011; Litter, 2015; Hao *et al.*, 2018; Niazi *et al.*, 2018a). Nguyen *et al.* (2008) investigated photocatalyst experiments with titanium dioxide (TiO₂) as the photocatalyst to remove arsenic. The results showed that 98% of arsenic could be reduced by photocatalysis reaction with TiO₂ from water containing 500 µg/L of arsenic. Kumar and Quaff used a commercial coagulant (ferric chloride, FeCl₃) to study arsenic removal by a coagulation–flocculation method and the maximum removal efficiency of arsenic reached 69.25% at 40 mg/L concentration of FeCl₃ (Kumar & Quaff 2019). The arsenic

This is an Open Access article distributed under the terms of the Creative Commons Attribution Licence (CC BY 4.0), which permits copying, adaptation and redistribution, provided the original work is properly cited (<http://creativecommons.org/licenses/by/4.0/>).

removal from aqueous solution by electrochemical means was studied, and almost 95% was removed within 5 min from the initial concentration of 10 mg/L (Lakshmipathiraj *et al.* 2010). However, the disadvantages of these processes are still significant, including high operational cost, strict operational requirement and insufficient removal for low-concentration arsenic-polluted water (Xu *et al.* 2019; Amen *et al.* 2020). In recent years, adsorption technology has been considered as a promising arsenic removal method for water, due to its low cost, high efficiency and no sludge production (Niazi *et al.* 2018b). Table 1 lists the studies on arsenic removal through adsorption. Therefore, in this research, adsorption technology was selected for arsenic removal from aqueous solutions.

Red mud is a fine-grained residue discarded in alumina production. When 1 ton of alumina is produced, approximately 1–1.5 tons of red mud residues are produced (Chen *et al.* 2018). At this time, the main disposal of red mud is through stack and landfill, which not only occupies a lot of land resources, but also has great potential harm to the environment. Therefore, proper disposal of red mud has attracted more attention. Red mud is applied to adsorption in many research studies, because red mud has a porous structure and its surface carries hydroxyl groups (Wu *et al.* 2017). Li *et al.* investigated the adsorptive removal of diclofenac and phosphate from aqueous solutions onto pyrrole-modified red mud by an in-situ chemical oxidative polymerization method (Li *et al.* 2020). Yunus *et al.* explored the adsorption capacity of fluoride in aqueous solution by red mud with acid modification and without modification (Cengelloglu *et al.* 2002). Neutralized red mud was used as an adsorbent to remove arsenic from water and the removal rate reached above 90% (Genç *et al.* 2003). These studies confirmed the possibility of red mud-based adsorbents.

In this research, novel red mud porous beads (RPB) were prepared by cross-linking sodium alginate with iron ions and used as an adsorbent to remove arsenic(V) from water. The major goals of this research were to: (1) study the adsorption capacity and evaluate the factors that affect the adsorption process on RPB, (2) investigate the adsorption performance and progress in column studies, and (3) investigate the mechanism of arsenic onto RPB.

MATERIALS AND METHODS

Materials

All chemicals used in this experiment were of analytical grade. The stock arsenic solution (1,000 µg/L) was prepared from a high concentration standard arsenic solution (Sinopharm Chemical Reagent, 100 mg/L). Red mud, collected from an aluminum company in Shandong province, was oven dried overnight at 60 °C and passed through a 40-mesh sieve. The chemical compositions of red mud were studied by X-ray fluorescence (XRF). The results are shown in Table 2.

Preparation of adsorbents

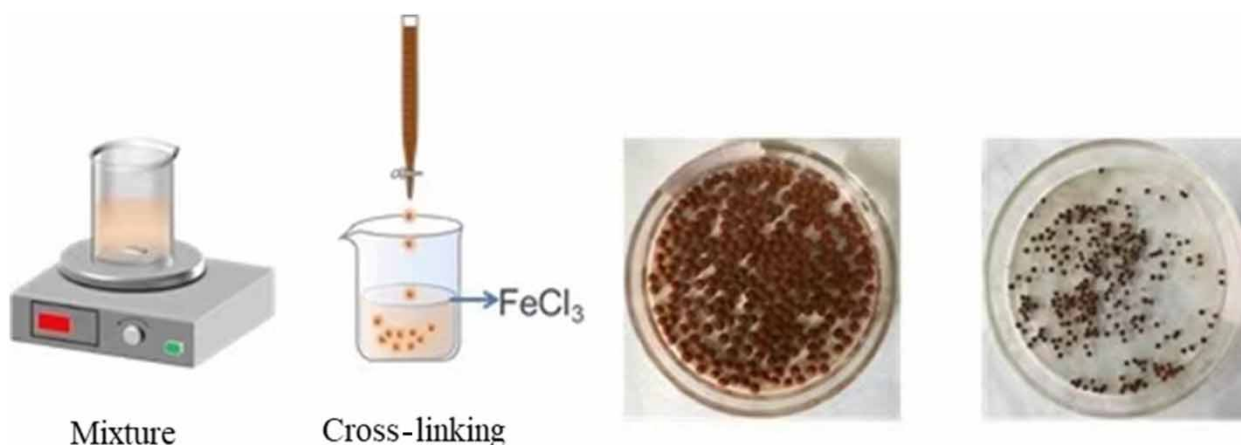
The red mud porous beads prepared in this study referred to the method of preparing of porous beads by Peretz *et al.* (2015). A brief description of porous beads synthesis is given below. The aqueous mixture of 3 g sodium alginate and 6% sodium chloride (NaCl) solution (6 g NaCl and 100 mL deionized water) was placed on a magnetic stirrer at 50 °C under continuous stirring (1,000 rpm) for 20 min. After that, 5 g red mud were added in it and stirring was continued (1,000 rpm) for 20 min. Thus, a homogenous mixture was obtained and the same was added as droplets into a 2.0% (w/w) ferric trichloride (FeCl₃) solution. The beads were then filtered, rinsed with deionized water 3–5 times to eliminate the surplus amount of FeCl₃, and then, beads were soaked in 0.5% (w/w) FeCl₃ for about 12–16 hours. The beads were washed with deionized water three times. After drying in an oven for 4 h at 60 °C, the beads were prepared successfully. The difference between the red mud porous beads (RPB) and red mud beads (RB) was whether NaCl was added. The schematic flowchart of preparation of RPB is presented in Figure 1.

Table 1 | Removal of arsenic by various adsorbents

Adsorbents	Arsenic valence state	Arsenic concentration	Removal rate (%)	References
Saxaul ash	As(V)	250 µg/L	94.62	Rahdar <i>et al.</i> (2019)
Zeolites	As(V)	10 mg/L	79.13	Kang <i>et al.</i> (2019)
Biochar	As(III), As(V)	4 mg/L	81, 84	Niazi <i>et al.</i> (2018b)
Red mud sludge	As(III)	2.5 mg/L	96	Naga Babu <i>et al.</i> (2021)

Table 2 | Main components of red mud (%)

Fe_2O_3	Al_2O_3	SiO_2	Na_2O	TiO_2	CaO
35.0	22.0	20.0	10.0	5.0	3.0

**Figure 1** | Preparation process of red mud porous beads.

Characterization of the adsorbents

The surface areas were measured via a surface area analyzer and calculated by the N_2 -Brunauer–Emmett–Teller (BET) method. The surface morphology of the adsorbents was determined by scanning electron microscopy (SEM) (SU8010, Hitachi, Japan). The elemental composition of RPB was evaluated by X-ray fluorescence (XRF, ZSX Primus II, Rigaku, Japan). Fourier transform infrared (FT-IR) spectra were detected using a Spectrum 2 instrument (PerkinElmer, German).

Batch experiments

Batch experiments were carried out to determine the arsenic removal capacity of RB and RPB. Briefly, 0.1 g adsorbent was added into a 100 mL conical flask, in which 1 mg/L arsenic solution was contained. The experiments were carried out at 25 °C with 50 mL arsenic solution in a thermostatic oscillator at 200 rpm for 2 h. The pH of arsenic aqueous was adjusted to 7 by using 0.1 M HCl or 0.1 M NaOH.

The equilibrium adsorption capacity (q_e , mg/g) and removal rate (R, %) were calculated from Equations (1) and (2), respectively as follows:

$$q_e = \frac{(C_0 - C_e) \times V}{m} \quad (1)$$

$$R = \frac{(C_0 - C_e)}{C_0} \times 100\% \quad (2)$$

where, C_0 is the initial concentration of arsenic solution (mg/L), C_e is the concentration of arsenic solution at equilibrium time (mg/L), V is the solution volume (L) and m is the adsorbent dosage (g).

Kinetic and isotherm study

Batch adsorption kinetic experiments were carried out in 100-mL conical flasks containing 50 mL arsenic aqueous with 0.1 g RPB adsorbent. The conical flasks were put in a thermostatic oscillator at 200 rpm under constant temperature (25 °C). The samples were extracted, filtered and analyzed for the arsenic concentration at different time intervals (from 1 to 120 min). The sorption kinetics of arsenic were investigated using pseudo-first-order kinetic, pseudo-second-order kinetic and intra-particle diffusion models.

The experimental data were fitted with pseudo-first-order kinetic, pseudo-second-order kinetic and intra-particle diffusion models given as Equations (3)–(5), respectively:

$$\ln(q_e - q_t) = \ln q_e - K_1 t \quad (3)$$

$$\frac{t}{q_t} = \frac{1}{K_2 q_e^2} + \frac{t}{q_e} \quad (4)$$

$$q_t = K t^{\frac{1}{2}} + C \quad (5)$$

where, q_t (mg/g) is the arsenic adsorption at any time intervals, while K_1 (min^{-1}), K_2 ($\text{g}/(\text{mg min})$) and K are the adsorption rate constant of pseudo-first-order, pseudo-second-order and intra-particle diffusion models, respectively.

The sorption isotherm experiments were conducted at a constant temperature (25 °C) and at pH = 7. Accurately, 0.1 g of RPB adsorbent was added into the 100-mL conical flasks containing 50 mL arsenic aqueous, the initial concentration ranged from 1 to 20 mg/L. The experimental data were fitted with the Langmuir isotherm and Freundlich isotherm. The Langmuir isotherm and the Freundlich isotherm are based on a monolayer adsorption assumption and the multilayer adsorption condition, respectively (Zhu *et al.* 2016).

The Langmuir isotherm and the Freundlich isotherm were calculated from Equations (6) and (7), respectively:

$$q_e = \frac{q_m K_L C_e}{1 + K_L C_e} \quad (6)$$

$$q_e = K_F C_e^{\frac{1}{n}} \quad (7)$$

where, q_m is the theoretical maximum adsorption capacity (mg/g), K_L and K_F are the Langmuir constant (L/mg) and Freundlich constant (mg/g), respectively. In order to calculate the adsorption efficiency of the adsorption process and know whether the adsorption process is favorable or unfavorable for the Langmuir type adsorption, the dimensionless factor R_L was defined by Equation (8):

$$R_L = \frac{1}{1 + K_L C_0} \quad (8)$$

The R_L value indicates whether the adsorption process is favorable or unfavorable at a certain concentration. When $R_L > 1$, it presents that the adsorption process to be unfavorable; when $0 < R_L < 1$, the adsorption process is favorable; when $R_L = 0$, the adsorption process is irreversible; when $R_L = 1$, the adsorption process is linear (Shao *et al.* 2019).

Effect of pH and adsorbent dosage

To determine the effect of pH, the arsenic initial concentrations for 1 mg/L were adjusted to different pH levels from 3 to 12. Here, 50 ml arsenic solutions with different pH were added into a flask with 0.1 g RPB. The mixed solution was stirred for 2 h to reach the equilibrium. The point of zero charge (pH_{pzc}) was also determined using the potentiometric mass titration method (Koh *et al.* 2020). The surface charge of adsorbent was negative at $\text{pH} > \text{pH}_{\text{pzc}}$ and positive at $\text{pH} < \text{pH}_{\text{pzc}}$ (Kragović *et al.* 2019). Briefly, 100 ml 0.01 mol/L sodium nitrate (NaNO_3) was added into a flask with 1 g/L RPB. The pH of NaNO_3 was adjusted to 3–12 by 0.1 M HCl or 0.1 M NaOH. The flasks were put in a thermostatic oscillator at 200 rpm for 2 h under constant temperature (25 °C). The final pH was measured and the changes of pH (ΔpH) were depicted against the initial pH. The point where the change of pH was zero was the pH_{pzc} .

In order to evaluate the effect of adsorbent dosage, the adsorbent dosage of 1–5 g/L was added into the arsenic solution with initial concentration of 5 mg/L. Other experimental steps were the same as those in the pH study.

Column experiments

An adsorption column apparatus was constructed to perform fixed bed column studies for the adsorption of arsenic into RPB. The fixed bed column experiment was conducted by using a laboratory-scale column with an inner diameter of 30 mm and a height of 100 mm. The solution was passed through the column upward. An adsorbent height of 3 cm was fixed in all experiments. The bed volume of the column was 21.195 cm^3 . The schematic flowchart of the column experiment is shown in

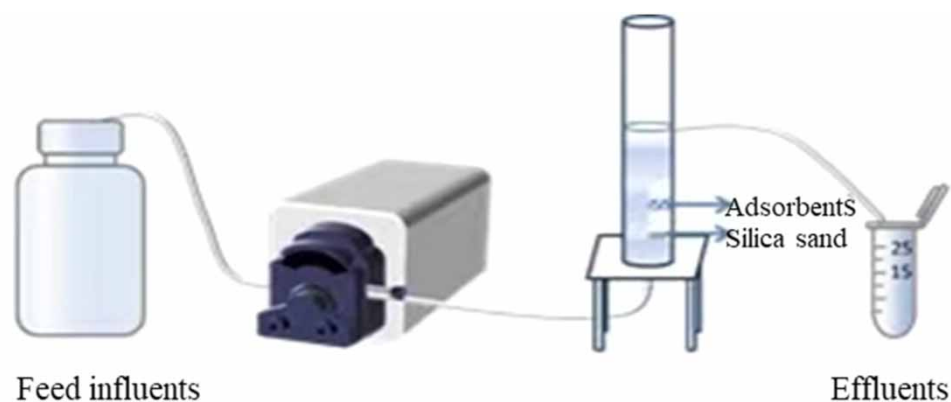


Figure 2 | Schematic flowchart of column experiments.

Figure 2. All the experiments were carried out at room temperature about 20 °C and initial pH at 7. In this study, different arsenic concentrations (1, 5 mg/L) at neutral pH were passed through the column reactor at a specified flow rate (1, 5 mL/min) using a peristaltic pump. Effluent samples were taken from the head of the column reactor at regular time intervals. The Thomas model and the Yoon–Nelson model are expressed by Equations (9) and (10):

$$\ln\left(\frac{C_0}{C_t} - 1\right) = \frac{k_{th}q_{th}m}{Q} - k_{th}C_0t \quad (9)$$

$$\ln\left(\frac{C_t}{C_0 - C_t}\right) = k_{yn}t - t_h k_{yn} \quad (10)$$

where, k_{th} is the rate constant of Thomas model (mL/(mg min)), q_{th} is the maximum adsorption capacity of Thomas model (mg/g); k_{yn} is the rate constant of the Yoon–Nelson model (min^{-1}) and t_h is the time required to half the bed saturation (min).

RESULTS AND DISCUSSION

Characterization of adsorbents

The SEM images of RB and RPB are shown in [Figure 3\(a\)](#) and [3\(b\)](#), respectively. RB showed a smooth surface that was slightly crumpled, while RPB had more gills and more obvious pores on its surface. These results indicated that the RPB was a porous bead and might be a good adsorbent for wastewater treatment. The BET surfaces of RB and RPB were 6.75 and 18.52 m²/g, respectively. The result confirmed that the RPB had a larger surface than RB as the average pore size increased from 21.0 to 24.9. The FTIR spectra of RB and RPB are presented in [Figure 3\(c\)](#). The presence of bands at 2,920 cm⁻¹ and 2,851 cm⁻¹ presented in RPB were related to the symmetric stretching vibrations of aldehydic C–H groups in the adsorbent ([Naga Babu et al. 2021](#)). In addition, the bands at 3,458 and 3,425 cm⁻¹ were attributed to the stretching vibration of O–H, indicating that RPB increased more O–H functional groups than red mud. The effect of time on adsorption of arsenic from water by RPB and RB was investigated under the initial concentration of 1 mg/L. The result is presented in [Figure 3\(d\)](#). The reaction between arsenic solution and adsorbents achieved equilibrium at 90 min and removal rate reached 90 and 77%, respectively. The result showed that RPB had the higher removal rate than RB. From [Table 3](#), it can be seen that the adsorbent of RPB was composed of 73.0% of Fe₂O₃ and 7.6% of Al₂O₃. Compared with the components of red mud, the content of Fe₂O₃ obviously increased, confirming that iron was successfully impregnated into RPB.

Effect of pH and dosage

The pH of the solution played an important role in the adsorption process because the surface charge was changed under different pH conditions ([Rahman et al. 2020](#)). The point of zero charge (pH_{pzc}) and effect of the pH on adsorption process were studied. From [Figure 4](#), it can be seen that the pH_{pzc} is at 6.0. When the solution pH was < 6.0, the surface of the adsorbent had a positive charge, which would accelerate the adsorption process. When the pH is > 6.0, the surface of the adsorbent turned into negatively charged, which would have adverse impacts on the adsorption progress due to electrostatic repulsion

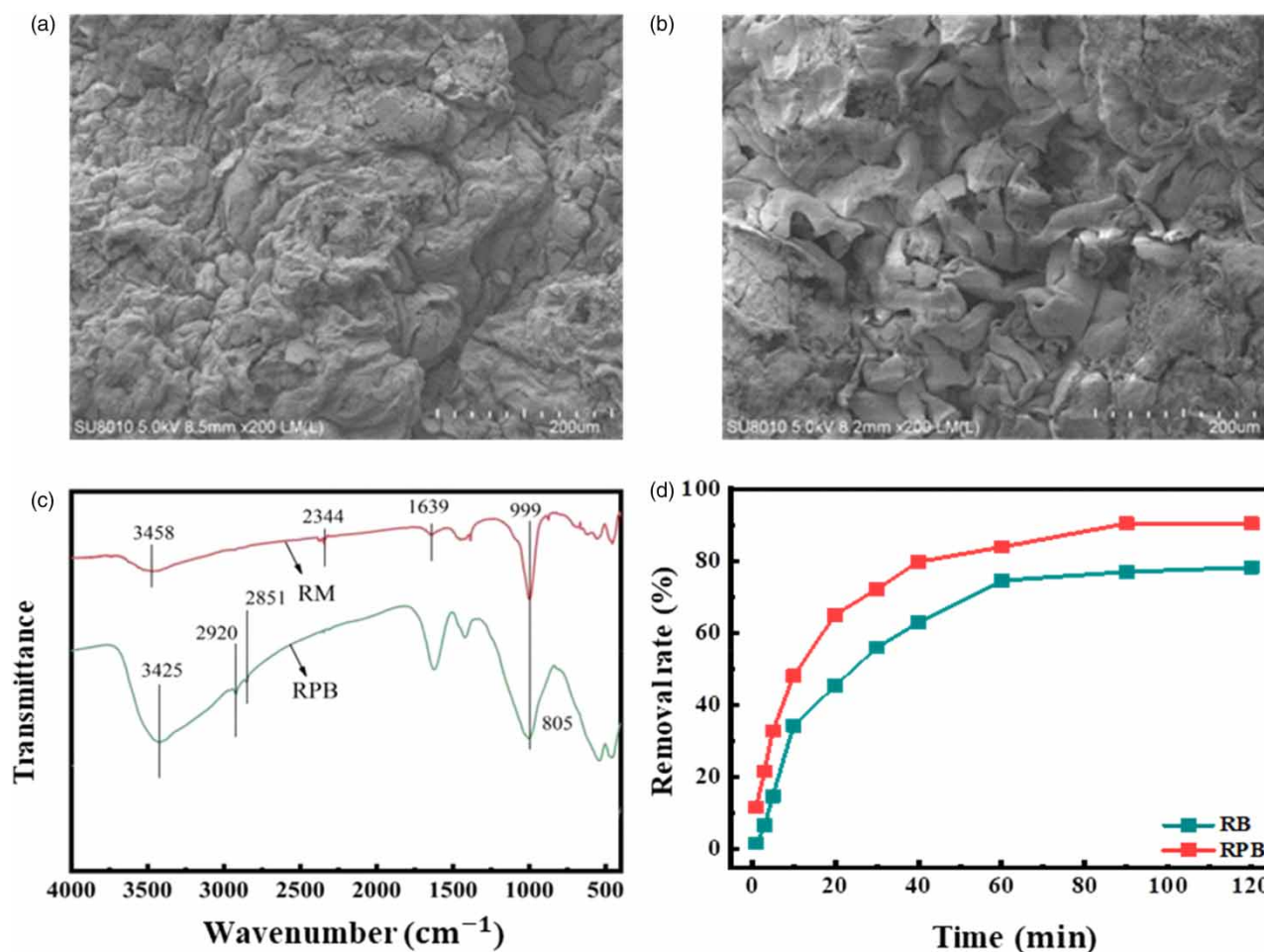


Figure 3 | SEM images (a, b), FTIR spectra (c) and arsenic removal rate (d) of RB and RPB.

Table 3 | Main components of RPB (%)

Fe ₂ O ₃	Al ₂ O ₃	TiO ₂	SiO ₂	Cl	P ₂ O ₅	SO ₃	Na ₂ O
73.0	7.6	6.0	4.8	3.2	2.4	2.0	0.2

(Yin *et al.* 2021). When pH was ≤ 6 , the removal rate of the arsenic from aqueous solution reached nearly 100%. The removal rate of arsenic first increased (pH = 4) and then decreased with the increase in pH. Especially at pH of 12, arsenic adsorption performance completely deteriorated with nearly 0 of arsenic removed. The form of the arsenic under this situation was negatively charged AsO_4^{3-} , while the surface of the adsorbent was also negatively charged after a pH of 6; this led to a greater repulsion between the adsorbate and adsorbent, which deteriorated the arsenic adsorption behavior.

Figure 5 depicts the effect of adsorbent dosage on arsenic removal rate and adsorption capacity. The diagram indicated that with the increase in adsorbent dosage from 1 g/L to 5 g/L, the removal rate increased from 62.6% to 92.3%. This could be explained by the increasing active sites on the RPB surface and greater surface area of RPB (Rahman *et al.* 2020; Yin *et al.* 2021). However, the adsorbent capacity reduced from 3.13 to 0.92 mg/g with the adsorbent dosage increasing from 1 to 5 g/L. The increase in adsorption capacity was due to the larger surface area and greater number of adsorption sites available that were introduced by increasing the number of particles. Considering the adsorption efficiency and economics, we chose the adsorbent dosage of 2 g/L in kinetic and isotherm studies.

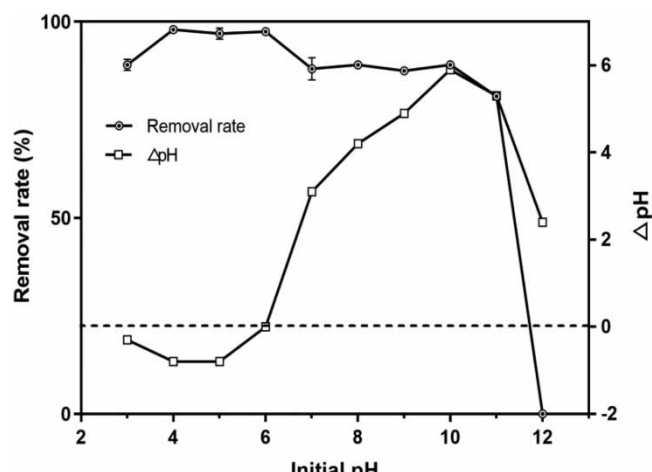


Figure 4 | The point of zero charge and effect of pH on RPB.

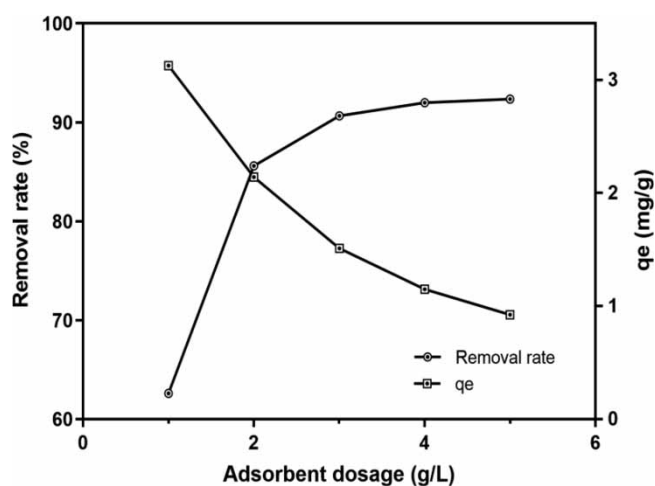


Figure 5 | Effect of the dosage of RPB on arsenic removal rate and adsorption capacity.

Adsorption kinetics

As shown in Figure 6, the effect of time was studied under initial concentrations of 1, 5 and 10 mg/L. The data were fitted by pseudo-first-order and pseudo-second-order models at optimum physicochemical parameters of pH at 7, dosage of 2 g/L, and temperature at 25 °C. The kinetic parameters determined from the rate models are presented in Figure 6 and Table 4.

It was clearly seen that the correlation coefficient of the pseudo-second-order kinetics model was higher than that of the pseudo-first-order kinetics model, and the calculated equilibrium adsorption capacity ($q_{e,cal}$) of the pseudo-second-order kinetics model was in agreement with the experimental data. Hence, the pseudo-second-order kinetics model was suitable to describe the adsorption of arsenic for the entire adsorption period. The results assumed that chemical adsorption was the controlling step and the adsorption rate was directly proportional to the square of the unoccupied adsorption sites on the surface of the adsorbent as well as the concentration of the arsenic. The equilibrium adsorption capacity increased with the increase in the initial concentration. The adequate adsorptive sites and driving force of greater concentration gradients may lead to the initial rapidly increased adsorption capacity.

Meanwhile, the intra-particle diffusion model was also applied to evaluate the rate limiting steps involved in the kinetic mechanism. The plots of q_t versus $t^{0.5}$ are shown in Figure 7 under three different concentrations of arsenic. The adsorption mechanism generally included three steps: (I) film diffusion (II) intra-particle diffusion or pore diffusion on the surface (III) adsorption onto interior sites. From Figure 7 it could be seen that all the three linear plots did not pass through the origin,

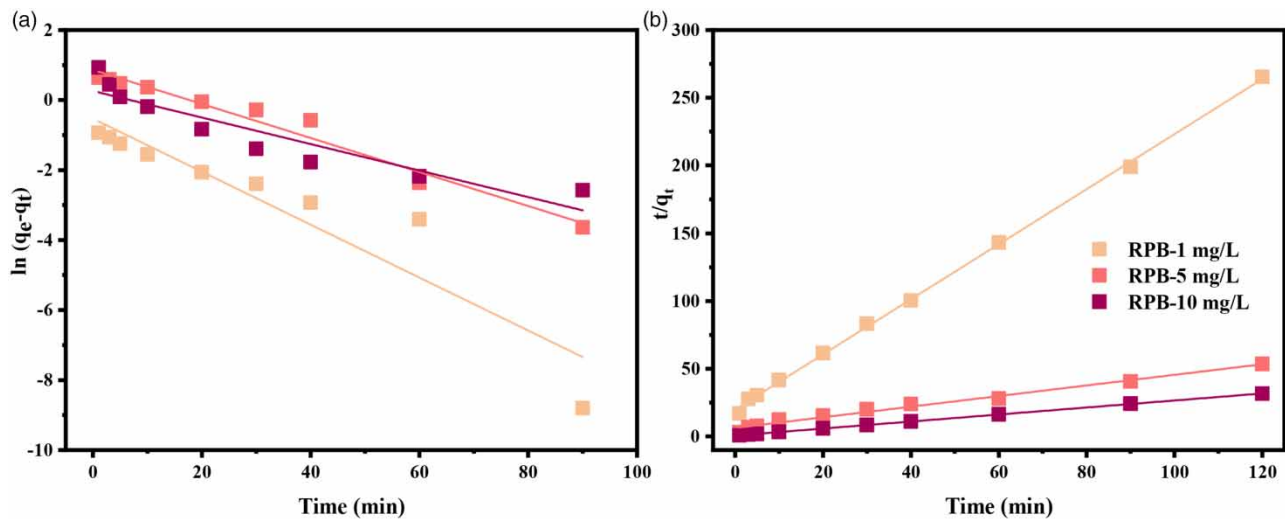


Figure 6 | Pseudo-first-order and pseudo-second-order fitting with arsenic concentrations of 1, 5 and 10 mg/L.

Table 4 | Kinetic parameters of pseudo-first-order and pseudo-second-order

C ₀ (mg/L)	q _e (mg/g)	Pseudo-first-order constant			Pseudo-second-order constant		
		q _e (mg/g)	k ₁ (1/min)	R ²	q _e (mg/g)	k ₂ (g/mg/min)	R ²
1	0.45	0.59	0.174	0.8769	0.49	0.208	0.9991
5	2.24	2.37	0.112	0.9698	2.55	0.024	0.9921
10	3.80	1.30	0.087	0.8674	3.86	0.104	0.9998

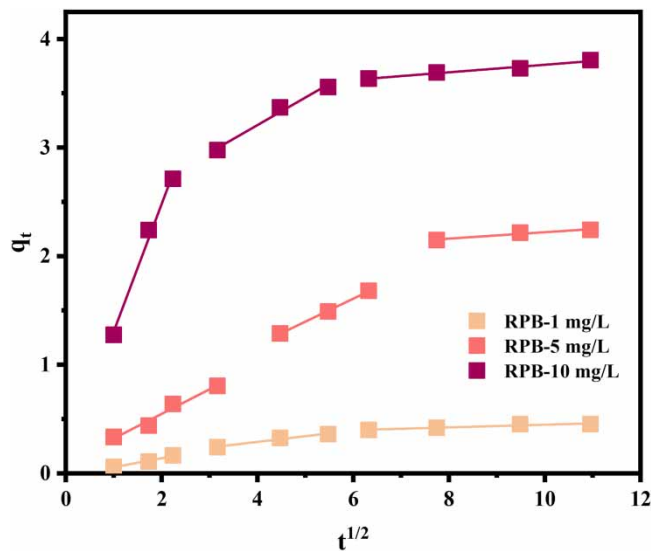


Figure 7 | Intra-particle diffusion model for adsorption of arsenic.

which illustrated that intra-particle diffusion was not the only rate controlling step in the adsorption process and some other mechanisms might be referred to the process. The initial rapid removal of arsenic may be governed by boundary layer diffusion and the subsequent slow uptake was attributed to the intra-particle pore diffusion effect (Gupta & Ghosh 2009). The rate

constant (K_i) and the corresponding correlation coefficients, determined from the intra-particle diffusion model at three different concentrations, are displayed in Table 5.

Adsorption isotherms

The adsorption isotherm revealed the distribution of adsorbed molecules in the liquid phase and solid phase when the adsorption process achieved an equilibrium state (Peng *et al.* 2014). The data were fitted by the Langmuir isotherm and the Freundlich isotherm (Figure 8). The isotherm constants and R^2 values for each model are given in Table 6. The R^2 value of the Langmuir isotherm was higher than that of the Freundlich isotherm, which indicated that the adsorption data were fitted better with the Langmuir isotherm. It was indicated that the adsorption of arsenic onto the adsorbent surface was a monolayer sorption process. The calculated R_L value found in this study was 0.6560, between zero and one, representing a favorable adsorption process of RPB. The absorption capacity of red mud is about 0.55–0.60 mg/g, which is consistent with other work done before (Li *et al.* 2010). In this study, the maximum adsorption capacity is 11.76 mg/g, larger than the reported value.

Effect of initial concentration

As depicted in Figure 9, the removal rate and adsorption capacity were significantly impacted by the initial concentration of arsenic. The removal rate was decreased from 91.3% to 79.0% with the increased initial concentration of arsenic from 2.5 to 20 mg/L. This might be attributed to the delayed establishment of equilibrium between the adsorbent sites and the arsenic in aqueous phase due to the increase in initial arsenic concentrations. But the adsorption capacity of the adsorbent increased with the initial concentration of arsenic. This discrepancy in behavior was due to the increase in concentration gradient of arsenate between the sorption sites and in the aqueous phase.

Table 5 | Intra-particle diffusion constants and correlation coefficients for adsorption of arsenic

C_0 (mg/L)	First step			Second step			Third step		
	K_i (mg/g/min ^{0.5})	C	R^2	K_i (mg/g/min ^{0.5})	C	R^2	K_i (mg/g/min ^{0.5})	C	R^2
1	0.084	−0.029	0.9800	0.053	0.079	0.9760	0.012	0.323	0.9131
5	0.227	0.094	0.9701	0.211	0.340	0.9990	0.030	1.925	0.9612
10	1.173	0.133	0.9920	0.254	2.193	0.9837	0.035	3.415	0.9743

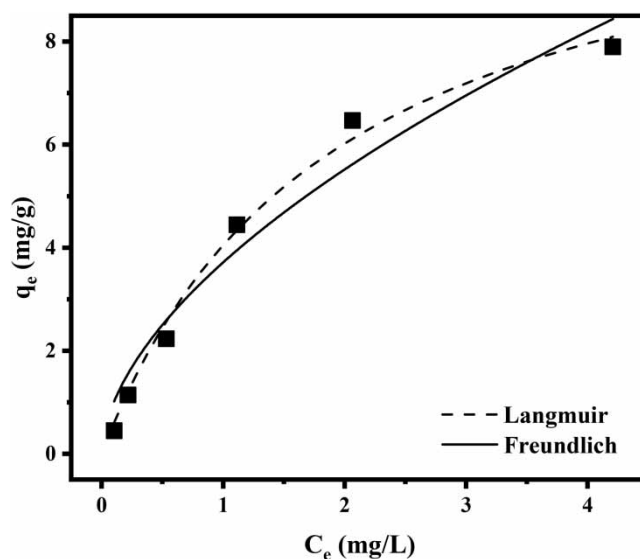
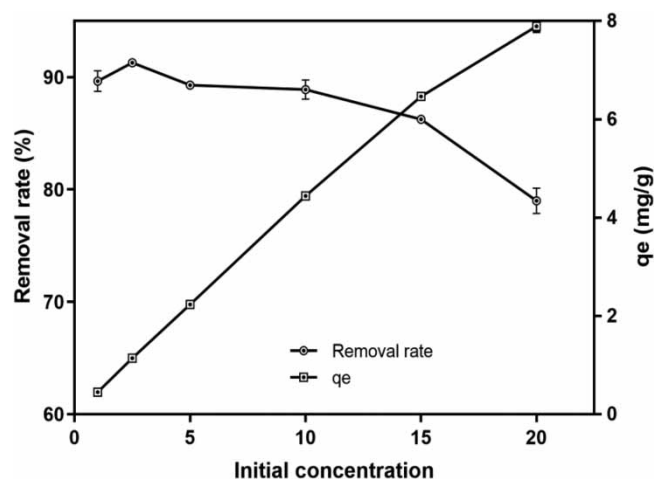


Figure 8 | Langmuir and Freundlich isotherms for adsorption of arsenic.

Table 6 | Langmuir and Freundlich isotherm parameters

Langmuir constant				Freundlich constant		
q_{\max} (mg/g)	K_L (L/mg)	R^2	R_L	$1/n$	K_F (mg/g)	R^2
11.76	0.52	0.9930	0.6560	0.57	3.71	0.9583

**Figure 9** | Effect of initial concentration of arsenic.

Column experiments

The measured experimental break through curve for the adsorption of arsenic is presented in Figure 10. The breakthrough points were 2.2, 23.8, 39.2 and 60.2 bed volume (BV) at 5 mg/L, 1 mL/min, 5 mg/L, 0.5 mL/min, 1 mg/L, 1 mL/min and 1 mg/L, 0.5 mL/min, respectively (according to $C/C_0 = 0.1$). The breakthrough point for the 5 mg/L solution appeared more quickly than that for the 1 mg/L solution. That might be interpreted as mass transfer limitations and/or chemical kinetics. The breakthrough time for the velocity of flow of 1 mL/min was faster than that for 0.5 mL/min, because more RPB was fed to the column unit interval (Santos *et al.* 2019). This meant that the exposure of arsenic to the active sites was reduced with the fluid superficial velocity increasing. The initial concentration of arsenic and the different velocities of flow caused the limitations to reach the break through curve (Baek *et al.* 2007). The parameters of the Thomas and Yoon–Nelson models were

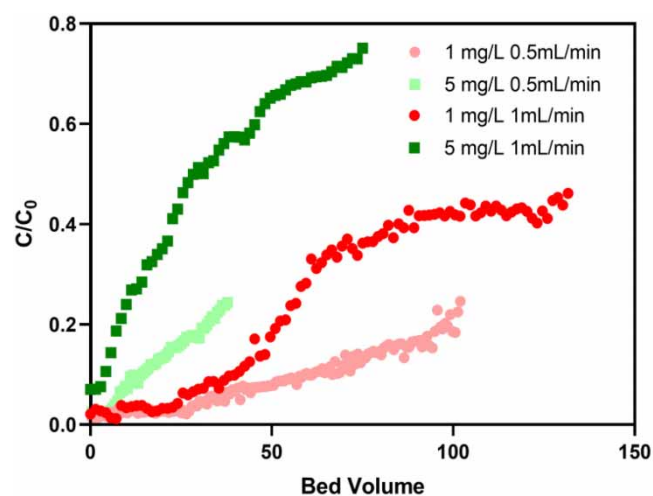
**Figure 10** | Break through curve for the adsorption of arsenic.

Table 7 | Fixed parameters of the Thomas model and the Yoon–Nelson models

	Thomas model			Yoon–Nelson model		
	k_{th} (mL/(mg min))	q_{th} (mg/g)	R^2	k_{yn} (min ⁻¹)	t_h (min)	R^2
1 mg/L 0.5 mL/min	0.65	1.52	0.9504	0.65×10^{-3}	6,092	0.9504
1 mg/L 1 mL/min	1.44	1.19	0.8549	1.44×10^{-3}	2,375	0.8549
5 mg/L 0.5 mL/min	0.34	2.59	0.8707	1.72×10^{-3}	2,052	0.8707
5 mg/L 1 mL/min	0.39	2.08	0.8660	1.96×10^{-3}	826	0.8660

summarized in Table 7. From Table 7, it was found that k_{th} and q_{th} increased for higher initial concentration and lower velocity of flow for the Thomas model. An increase in both the initial concentration and the flow rate led to an increase in k_{yn} and a decrease in t_h for the Yoon–Nelson model. This is because column saturation is reached more quickly at a higher initial arsenic concentration and flow rate (Jang & Sung 2019).

CONCLUSION

In this research, the adsorption of arsenic onto the RPB was studied through batch experiments and column studies. The removal rate of arsenic onto RPB was higher than that onto RB, and reached 90 and 77% respectively. The adsorption process was governed by chemisorption. The data fitted better with the Langmuir isotherm, indicating that the adsorption of arsenic onto the adsorbent surface was a monolayer sorption process. The adsorption capacity inferred from the Langmuir isotherm was 11.758 mg/g under 25 °C. The pH_{pzc} is at 6.0, and when $pH > 6.0$, the removal efficiency of arsenic decreased. When the initial concentration of arsenic was 2.5 mg/L, the removal rate of arsenic was the maximum at 95%. With the initial concentration increasing, the removal rate decreased. With the increase in adsorbent dosage from 1 g/L to 5 g/L, the removal rate increased from 62.6% to 92.3%, while the adsorbent capacity reduced from 3.13 to 0.92 mg/g. According to the column studies, increasing velocity of flow and initial concentrations significantly promoted the saturation of the adsorption column. In short, RPB showed a high arsenic adsorption capacity and can act as a facile and cost-effective adsorbent for adsorption in a future field test.

ACKNOWLEDGEMENT

This study was funded by the Major Science and Technology Innovation Project of Shandong Province (Grant No. 2018YFJH0902).

DECLARATION OF INTEREST STATEMENT

The authors declare that there is no conflict of interest regarding the publication of this paper.

DATA AVAILABILITY STATEMENT

Data cannot be made publicly available; readers should contact the corresponding author for details.

REFERENCES

- Akin, I., Arslan, G., Tor, A., Ersoz, M. & Cengelloglu, Y. 2012 Arsenic(V) removal from underground water by magnetic nanoparticles synthesized from waste red mud. *Journal of Hazardous Materials* **235–236**, 62–68. <http://dx.doi.org/10.1016/j.jhazmat.2012.06.024>.
- Amen, R., Bashir, H., Bibi, I., Shaheen, S. M., Niazi, N. K., Shahid, M., Hussain, M. M., Antoniadis, V., Shakoar, M. B., Al-Solaimani, S. G., Wang, H., Bundschuh, J. & Rinklebe, J. 2020 A critical review on arsenic removal from water using biochar-based sorbents: the significance of modification and redox reactions. *Chemical Engineering Journal* **396**, 125195.
- Baek, K. W., Song, S. H., Kang, S. H., Rhee, Y. W., Lee, C. S., Lee, B. J., Hudson, S. & Hwang, T. S. 2007 Adsorption kinetics of boron by anion exchange resin in packed column bed. *Journal of Industrial and Engineering Chemistry* **13** (3), 452–456.
- Bilici Baskan, M. & Pala, A. 2010 A statistical experiment design approach for arsenic removal by coagulation process using aluminum sulfate. *Desalination* **254** (1–3), 42–48.
- Cengelloglu, Y., Kir, E. & Erso, M. 2002 Removal of fluoride from aqueous solution by using red mud. *Separation and Purification Technology* **28**, 81–86.

- Chen, S., Zhu, Q., Su, Y. & Xing, Z. 2018 Preparation and performance of Fe(II)-akaganeite(β -FeOOH) modified red mud granule filter material. *Research on Chemical Intermediates* **44** (12), 7583–7593. <https://doi.org/10.1007/s11164-018-3575-x>.
- Genç, H., Tjell, J. C., McConchie, D. & Schuiling, O. 2003 Adsorption of arsenate from water using neutralized red mud. *Journal of Colloid and Interface Science* **264** (2), 327–334.
- Gupta, K. & Ghosh, U. C. 2009 Arsenic removal using hydrous nanostructure iron(III)-titanium(IV) binary mixed oxide from aqueous solution. *Journal of Hazardous Materials* **161** (2–3), 884–892.
- Hao, L., Wang, N., Wang, C. & Li, G. 2018 Arsenic removal from water and river water by the combined adsorption – UF membrane process. *Chemosphere* **202**, 768–776.
- Jang, J. & Sung, D. 2019 Effective phosphorus removal using chitosan/Ca-organically modified montmorillonite beads in batch and fixed-bed column studies. *Journal of Hazardous Materials* **375** (April), 9–18. <https://doi.org/10.1016/j.jhazmat.2019.04.070>.
- Kang, S., Park, S. M., Park, J. G. & Baek, K. 2019 Enhanced adsorption of arsenic using calcined alginate bead containing alum sludge from water treatment facilities. *Journal of Environmental Management* **234** (December 2018), 181–188. <https://doi.org/10.1016/j.jenvman.2018.12.105>.
- Kim, J., Benjamin, M. M., Kwan, P. & Chang, Y. 2003 A novel ion exchange process for as removal. *Journal/American Water Works Association* **95** (3), 77–85.
- Koh, K. Y., Zhang, S. & Paul Chen, J. 2020 Hydrothermally synthesized lanthanum carbonate nanorod for adsorption of phosphorus: material synthesis and optimization, and demonstration of excellent performance. *Chemical Engineering Journal* **380** (July 2019), 122153. <https://doi.org/10.1016/j.cej.2019.122153>.
- Kragović, M., Stojmenović, M., Petrović, J., Lored, J., Pašalić, S., Nedeljković, A. & Ristović, I. 2019 Influence of alginate encapsulation on point of zero charge (pH pzc) and thermodynamic properties of the natural and Fe(III)-modified zeolite. *Procedia Manufacturing* **32**, 286–293. <https://doi.org/10.1016/j.promfg.2019.02.216>.
- Kumar, I. & Quaff, A. R. 2019 Comparative study on the effectiveness of natural coagulant aids and commercial coagulant: removal of arsenic from water. *International Journal of Environmental Science and Technology* **16** (10), 5989–5994. <https://doi.org/10.1007/s13762-018-1980-8>.
- Lakshmipathiraj, P., Prabhakar, S. & Raju, G. B. 2010 Studies on the electrochemical decontamination of wastewater containing arsenic. *Separation and Purification Technology* **73** (2), 114–121. <http://dx.doi.org/10.1016/j.seppur.2010.03.009>.
- Li, Y., Wang, J., Luan, Z. & Liang, Z. 2010 Arsenic removal from aqueous solution using ferrous based red mud sludge. *Journal of Hazardous Materials* **177** (1–3), 131–137. <http://dx.doi.org/10.1016/j.jhazmat.2009.12.006>.
- Li, X., Ji, M., Nghiem, L. D., Zhao, Y., Liu, D., Yang, Y., Wang, Q., Trinh, Q. T., Vo, D. V. N., Pham, V. Q. & Tran, N. H. 2020 A novel red mud adsorbent for phosphorus and diclofenac removal from wastewater. *Journal of Molecular Liquids* **303**, 112286. <https://doi.org/10.1016/j.molliq.2019.112286>.
- Litter, M. I. 2015 Mechanisms of removal of heavy metals and arsenic from water by TiO₂-heterogeneous photocatalysis. *Pure and Applied Chemistry* **87** (6), 557–567.
- Mazumder, D. N. G. 2008 Chronic arsenic toxicity & human health. *Indian Journal of Medical Research* **128** (4), 436–447.
- Mohammed Abdul, K. S., Jayasinghe, S. S., Chandana, E. P. S., Jayasumana, C. & De Silva, P. M. C. S. 2015a Arsenic and human health effects: a review. *Environmental Toxicology and Pharmacology* **40** (3), 828–846.
- Mohammed Abdul, K. S., Jayasinghe, S. S., Chandana, E. P. S., Jayasumana, C. & De Silva, P. M. C. S. 2015b Arsenic and human health effects: a review. *Environmental Toxicology and Pharmacology* **40** (3), 828–846. <http://dx.doi.org/10.1016/j.etap.2015.09.016>.
- Naga Babu, A., Raja Sree, T., Srinivasa Reddy, D., Suresh Kumar, G. & Krishna Mohan, G. V. 2021 Experimental and statistical analysis of As(III) adsorption from contaminated water using activated red mud doped calcium-alginate beads. *Environmental Technology (United Kingdom)* **42** (12), 1810–1825. <https://doi.org/10.1080/09593330.2019.1681520>.
- Nguyen, T. V., Vigneswaran, S., Ngo, H. H., Kandasamy, J. & Choi, H. C. 2008 Arsenic removal by photo-catalysis hybrid system. *Separation and Purification Technology* **61** (1), 44–50.
- Niazi, N. K., Bibi, I., Shahid, M., Ok, Y. S., Burton, E. D., Wang, H., Shaheen, S. M., Rinklebe, J. & Lüttge, A. 2018a Arsenic removal by perilla leaf biochar in aqueous solutions and groundwater: an integrated spectroscopic and microscopic examination. *Environmental Pollution* **232**, 31–41.
- Niazi, N. K., Bibi, I., Shahid, M., Ok, Y. S., Shaheen, S. M., Rinklebe, J., Wang, H., Murtaza, B., Islam, E., Farrakh Nawaz, M. & Lüttge, A. 2018b Arsenic removal by Japanese oak wood biochar in aqueous solutions and well water: investigating arsenic fate using integrated spectroscopic and microscopic techniques. *Science of the Total Environment* **621** (October 2017), 1642–1651. <https://doi.org/10.1016/j.scitotenv.2017.10.063>.
- Peng, X., Huang, D., Odoom-Wubah, T., Fu, D., Huang, J. & Qin, Q. 2014 Adsorption of anionic and cationic dyes on ferromagnetic ordered mesoporous carbon from aqueous solution: equilibrium, thermodynamic and kinetics. *Journal of Colloid and Interface Science* **430**, 272–282. <http://dx.doi.org/10.1016/j.jcis.2014.05.035>.
- Peretz, S., Anghel, D. F., Vasilescu, E., Florea-Spiroiu, M., Stoian, C. & Zgherea, G. 2015 Synthesis, characterization and adsorption properties of alginate porous beads. *Polymer Bulletin* **72** (12), 3169–3182.
- Rahdar, S., Taghavi, M., Khaksefidi, R. & Ahmadi, S. 2019 Adsorption of arsenic (V) from aqueous solution using modified saxaul ash: isotherm and thermodynamic study. *Applied Water Science* **9** (4), 1–9. <https://doi.org/10.1007/s13201-019-0974-0>.

- Rahman, H. L., Erdem, H., Sahin, M. & Erdem, M. 2020 Iron-incorporated activated carbon synthesis from biomass mixture for enhanced arsenic adsorption. *Water, Air, and Soil Pollution* **231** (1), 6.
- Saha, N., Bodrud-Doza, M., Islam, A. R. M. T., Begum, B. A. & Rahman, M. S. 2020 Hydrogeochemical evolution of shallow and deeper aquifers in central Bangladesh: arsenic mobilization process and health risk implications from the potable use of groundwater. *Environmental Earth Sciences* **79** (20), 1–18. <https://doi.org/10.1007/s12665-020-09228-4>.
- Santos, A. F., Arim, A. L., Lopes, D. V., Gando-Ferreira, L. M. & Quina, M. J. 2019 Recovery of phosphate from aqueous solutions using calcined eggshell as an eco-friendly adsorbent. *Journal of Environmental Management* **238** (February), 451–459. <https://doi.org/10.1016/j.jenvman.2019.03.015>.
- Shao, Q., Lu, M., Zhou, J., Zhu, Z. & Song, Y. 2019 Preparation of non-sintered fly ash filter (NSFF) for ammonia nitrogen adsorption. *Environmental Technology (United Kingdom)* **40** (15), 1988–1999. <https://doi.org/10.1080/09593330.2018.1435733>.
- Wan, W., Pepping, T. J., Banerji, T., Chaudhari, S. & Giammar, D. E. 2011 Effects of water chemistry on arsenic removal from drinking water by electrocoagulation. *Water Research* **45** (1), 384–392.
- WHO 2008 *Guidelines for Drinking-Water Quality*. World Health Organization, Geneva. Vol. 35(5), pp. 307–312.
- Wu, C., Huang, L., Xue, S. G., Huang, Y. Y., Hartley, W., Cui, M. q. & Wong, M. H. 2017 Arsenic sorption by red mud-modified biochar produced from rice straw. *Environmental Science and Pollution Research* **24** (22), 18168–18178.
- Xu, X., Huang, H., Zhang, Y., Xu, Z. & Cao, X. 2019 Biochar as both electron donor and electron shuttle for the reduction transformation of Cr(VI) during its sorption. *Environmental Pollution* **244** (Vi), 423–430. <https://doi.org/10.1016/j.envpol.2018.10.068>.
- Yin, Y., Xu, G., Li, L., Qiao, C., Xiao, Y., Ma, T. & Liu, C. 2021 Removal of inorganic arsenic from aqueous solution by Fe-modified ceramsite: batch studies and remediation trials. *Water Science and Technology* **83** (7), 1522–1534.
- Zhu, N., Yan, T., Qiao, J. & Cao, H. 2016 Adsorption of arsenic, phosphorus and chromium by bismuth impregnated biochar: adsorption mechanism and depleted adsorbent utilization. *Chemosphere* **164**, 32–40.

First received 26 October 2021; accepted in revised form 7 January 2022. Available online 22 January 2022